

A Conservative, Consistent All-Mach Method to Simulate Liquid Atomization in Supersonic Flows

Yue Ling^{*1}, Bo Zhang^{1,2}

¹Department of Mechanical Engineering, Baylor University, Waco, TX 76798, USA

²School of Mechanical Engineering, Georgia Institute of Technology, Atlanta, GA 30332, USA

*Corresponding author email: stanley_ling@baylor.edu

Abstract

Atomization of bulk liquids subjected to a supersonic flow is essential to applications such as liquid fuel injection in supersonic propulsion systems. Since high-level details are often difficult to measure in experiments, numerical simulation is an important alternative to shed light on the unclear physics. A detailed numerical simulation (DNS) of liquid atomization in supersonic flows will need to rigorously resolve the shock waves, the interfaces, and the interaction between the two. In the present study, a new simulation framework for compressible multiphase flows is proposed. The geometric volume-of-fluid (VOF) method is employed to advect the sharp interfaces. The convection fluxes of density, momentum, and energy are computed based on the VOF flux, to achieve an important mass-momentum-energy consistence. To suppress spurious oscillations near shocks, numerical diffusion is introduced in single-phase regions away from the interface. The contribution of pressure is incorporated using a projection method, so that the method can be used for flows of all Mach numbers. Different compressible interfacial multiphase flow problems, including the two-phase shocktube, Richtmyer-Meshkov instability (RMI), and shock-drop interaction have been used to test the present method. The linear single-mode RMI with finite Weber and Reynolds numbers are simulated. The simulation results agree very well with the linear stability theory, which clearly affirms the capability of the present method in capturing the viscous and capillary effects on shock-interface interaction.

Keywords

Direct numerical simulation; Shock-interface interaction; Richtmyer-Meshkov instability

Introduction

Atomization of bulk liquids subjected to a supersonic flow is essential to different applications such as lithotripsy, raindrop damage in supersonic flight, and liquid fuel injection in supersonic propulsion systems. Detailed numerical simulations (DNS), which fully resolves the sharp interfaces and the interaction between the interfaces and the shocks, are essential to the investigation of atomization, since it can provide the high-level details that are hard to diagnose in experiments, including the interfacial dynamics and instability, the shock-interface interaction, and the interfacial topology changes. Though DNS is generally focused on small-scale canonical problems due to the high computational cost, the high-fidelity simulation results are still crucial to the development of sub-grid physics- or data-based models, to enable coarse-mesh simulations of industrial problems of larger scales. To fully resolve compressible interfacial multiphase flows that arise from supersonic atomization, the governing conservation laws must be solved by numerical methods that can well capture the sharp interface, the shock waves, and the interaction between them. It is essential to conserve mass of each phase. Furthermore, the surface tension on interfaces must be modeled and calculated rigorously.

In previous studies of shock-interface interaction, the surface tension is ignored since the time scale of interest is much smaller than the capillary time scale [1, 2, 3]. For such cases, it is acceptable to ignore surface tension and to use diffused-interface methods. However, for problems that involve small interfacial length scales or topology changes due to liquid breakups, the

capillary time scale becomes comparable to the flow time scale, then the surface tension is important and must be rigorously incorporated in the simulation. DNS of compressible interfacial multiphase flows with surface tension is an emerging area, and only a few studies are available in the literature [4, 5, 6, 7, 8]. The recent progress on the diffused-interface methods in simulating compressible two-phase flows is reviewed by Saurel and Pantano [9]. An HLLC-based scheme that incorporates surface tension was developed by Garrick *et al.* [6]. The method was based on the five-equation model and a diffused-interface method. The liquid volume fraction was solved by the HLLC method along with an interface compression technique to avoid excessive smearing. To improve the accuracy in surface tension calculation, the method was then extended by the same authors using an algebraic VOF method, *i.e.*, the Tangent of Hyperbola for Interface Capturing (THINC) method [10], to resolve the sharp interfaces [5]. For both methods, the same balanced-force discretization was used for surface tension calculation. Fuster and Popinet have presented an all-Mach method for simulation of CIMF with surface tension [7]. The geometric VOF method was used to resolve the interface. The fluxes for the conservative variables are computed based on that for the volume fraction, therefore, the advection methods for momentum and mass are consistent. The method was used to simulate the collapse of an air bubble in liquid and a good agreement with experiment was achieved. A minor drawback of the method is the lack of sufficient treatment for shock capturing, as a result, the numerical oscillations near discontinuities are not sufficiently damped. More recently, Corot *et al.* [8] developed an ALE method for two-phase compressible flows with surface tension. When the interface deformation is small, the interface is tracked based on the Lagrangian framework, while the deformation becomes large, the method switches to the Eulerian representation of the interface and resolves the interface with the VOF method. The method is accurate but is also more complicated to use due to the addition of the Lagrangian step. The viscous effects are generally ignored in these simulations [4, 8].

The present study aims at extending the method of Fuster and Popinet (FP) to enable direct numerical simulation of compressible interfacial multiphase flows with interaction between shock waves and interfaces. The key advantages of the FP method, such as the geometric mass-momentum consistent VOF method for interface capturing, will be inherited. Additional numerical diffusion following the central upwind method of Kurganov and Tadmor [11] will be introduced to eliminate the numerical oscillations near the shocks or contact discontinuities. Different test problems are simulated to examine the capability of the present method in capturing shock-interface interaction and the resulting interfacial dynamics and instability when finite viscosity and surface tension are present.

Simulation methods

The two different phases are distinguished by a characteristic function χ . Generally we use $\chi = 1$ and 0 to represent the liquid and gas phases, respectively. The advection equation for χ is given as

$$\frac{\partial \chi}{\partial t} + u_i \frac{\partial \chi}{\partial x_i} = 0. \quad (1)$$

The fluid properties jump across the interface separating the two phases. The mean value of χ in a computational cell is defined as $f = \frac{1}{\Delta \Omega} \int_{\Omega} \chi dV$. which also represents the volume fraction of liquid ($\chi = 1$) in a cell. Similarly, $\hat{f} = 1 - f$ is the gas volume fraction.

The governing equations for the two-phase model can be written as

$$\frac{\partial f \rho_l}{\partial t} + \frac{\partial f \rho_l u_i}{\partial x_i} = 0, \quad (2)$$

$$\frac{\partial \hat{f} \rho_g}{\partial t} + \frac{\partial \hat{f} \rho_g u_i}{\partial x_i} = 0, \quad (3)$$

$$\frac{\partial f \rho_l u_i}{\partial t} + \frac{\partial f \rho_l u_i u_j}{\partial x_j} = -f \frac{\partial p}{\partial x_i} + f \frac{\partial \tau_{ij}}{\partial x_j} - f \sigma \kappa \frac{\partial f}{\partial x_i}, \quad (4)$$

$$\frac{\partial \hat{f} \rho_l u_i}{\partial t} + \frac{\partial \hat{f} \rho_l u_i u_j}{\partial x_j} = -\hat{f} \frac{\partial p}{\partial x_i} + \hat{f} \frac{\partial \tau_{ij}}{\partial x_j} + \hat{f} \sigma \kappa \frac{\partial f}{\partial x_i}, \quad (5)$$

$$\frac{\partial f E_l}{\partial t} + \frac{\partial f E_l u_i}{\partial x_i} = -f \frac{\partial p u_i}{\partial x_i} + f \frac{\partial \tau_{ij} u_i}{\partial x_j} + f \sigma \kappa \frac{\partial f u_i}{\partial x_i}, \quad (6)$$

$$\frac{\partial \hat{f} E_g}{\partial t} + \frac{\partial \hat{f} E_g u_i}{\partial x_i} = -\hat{f} \frac{\partial p u_i}{\partial x_i} + \hat{f} \frac{\partial \tau_{ij} u_i}{\partial x_j} - \hat{f} \sigma \kappa \frac{\partial f u_i}{\partial x_i}, \quad (7)$$

where the variables with subscripts $k = l, g$ denote the liquid (l) and the gas (g) phases, respectively, while the average properties for the gas-liquid mixture are denoted by variables without a subscript. Furthermore, ρ_k , u_k , and p_k represent density, velocity, and pressure for the phase k . The total energy is denoted by $E_k = \rho_k (e_k + u_{k,i} u_{k,i} / 2)$, where e_k is the internal energy. The stiffened equation of state in the Mie-Grüneisen form is used to close the system

$$\rho_k e_k = \frac{p_k + \gamma_k \Pi_{k,\infty}}{\gamma_k - 1}, \quad (8)$$

where γ_k and $\Pi_{k,\infty}$ are the specific heat ratio and the reference pressure for the phase k . The values of γ_k and $\Pi_{\infty,k}$ for a given material are obtained by fitting the corresponding shock compression experimental data [12].

The momentum and energy equations for the mixture can be obtained by summing Eqs. (4)-(5), and Eqs. (6)-(7), respectively,

$$\frac{\partial \rho u_i}{\partial t} + \frac{\partial \rho u_i u_j}{\partial x_j} = -\frac{\partial p}{\partial x_i} + \frac{\partial \tau_{ij}}{\partial x_j} + \sigma \kappa \frac{\partial f}{\partial x_i}, \quad (9)$$

$$\frac{\partial \rho E}{\partial t} + \frac{\partial \rho E u_i}{\partial x_i} = -\frac{\partial p u_i}{\partial x_i} + \frac{\partial \tau_{ij} u_i}{\partial x_j} + \sigma \kappa u_i \frac{\partial f}{\partial x_i}. \quad (10)$$

The internal energy equation for the mixture can be obtained by subtracting the kinetic energy portion from Eq. (10) and is rewritten in terms of pressure as

$$\frac{1}{\rho c_{\text{eff}}^2} \left(\frac{\partial p}{\partial t} + u_i \frac{\partial p}{\partial x_i} \right) - \frac{\beta_T \Phi_\nu}{\rho C_p} = -\frac{\partial u_i}{\partial x_i}, \quad (11)$$

where β_T and C_p are the thermal expansion coefficient and specific heat for constant pressure. The effective sound speed c_{eff} is defined as

$$\frac{1}{\rho c_{\text{eff}}^2} = \frac{\gamma}{\rho c^2} - \frac{\beta_T^2 T}{\rho C_p}, \quad (12)$$

where T is the temperature and C_p is the specific heat for constant pressure. For both liquid and gas, it can be approximated that $1/\rho c_{\text{eff}}^2 \approx 1/\rho c^2$ [7].

Numerical Methods

The model equations are solved by the finite volume approach on a collocated grid. The advection equation for the characteristic function, Eq. (1) is discretized and solved using the geometric VOF method [13]. The convection terms for mass, momentum, and energy equations are handled for each phase separately, based on Eqs. (2)-(7). It has been demonstrated in previous studies that solving the mass (VOF) and momentum equations consistently is critical to yield accurate results for two-phase flow with large density contrast [14]. The conservative variables for each phase are advected as tracers associated with the volume fraction of the corresponding phase non-diffusively. Similar to the VOF method, the discretization for the convection terms is strictly conservative.

The fluxes for the conservative variables for the liquid, *i.e.*, $\mathbf{U}_l^n = [f\rho_l, f(\rho u_i)_l, fE_l]^n$ and for the gas, *i.e.*, $\mathbf{U}_g^n = [\hat{f}\rho_g, \hat{f}(\rho u_i)_g, \hat{f}E_g]^n$, are computed based on the f and \hat{f} fluxes,

$$\mathbf{F}_{U_l, j+1/2}^n = \mathbf{U}_{la, j}^n F_{f, j+1/2}^n, \quad \mathbf{F}_{U_g, j+1/2}^n = \mathbf{U}_{ga, j}^n F_{\hat{f}, j+1/2}^n, \quad (13)$$

where $F_{f, j+1/2}^n$ and $F_{\hat{f}, j+1/2}^n$ are the VOF fluxes for the liquid and gas volume fractions f and \hat{f} . The values of the conservative variables to be advected across the cell surface for the liquid and gas phases, *i.e.*, $\mathbf{U}_{la, j}^n$ and $\mathbf{U}_{ga, j}^n$, are computed by linear reconstruction of the corresponding variable within the j cell based on the Bell-Colella-Glaz scheme [15] and the minmod slope limiter. Then the conservative variables for each phase over time similar to the VOF function,

$$\Delta\Omega \frac{U_l^* - U_l^n}{\Delta t} = \Delta_i \mathbf{F}_{U_l, i}^n, \quad \Delta\Omega \frac{U_g^* - U_g^n}{\Delta t} = \Delta_i \mathbf{F}_{U_g, i}^n, \quad (14)$$

where $\Delta_i \mathbf{F}_{U_l, i}^n$ and $\Delta_i \mathbf{F}_{U_g, i}^n$ are the sums of net fluxes in all directions and the superscript * represent the updated variables after the convection step. The net fluxes in the x direction are calculated as

$$\Delta_x \mathbf{F}_{U_l, x}^n = \mathbf{F}_{U_l, j+1/2}^n - \mathbf{F}_{U_l, j-1/2}^n, \quad \Delta_x \mathbf{F}_{U_g, x}^n = \mathbf{F}_{U_g, j+1/2}^n - \mathbf{F}_{U_g, j-1/2}^n. \quad (15)$$

Numerical diffusion is introduced to damp the spurious oscillations generated, following the central method of Kurganov and Tadmor (KT) [11]. The numerical diffusion is applied only in the cells without interfaces ($f = 0$ or $f = 1$), so there is no smearing of properties at the sharp interface. The numerical diffusion fluxes are incorporated as

$$\Delta\Omega \frac{U^{**} - U^*}{\Delta t} = \Delta_i \mathbf{H}_i^n \quad \text{if } f = 0 \text{ or } f = 1, \quad (16)$$

where $\Delta_i \mathbf{H}_i^n$ is the sum of net numerical-diffusion fluxes in all directions, and U^{**} represents the variables after the numerical-diffusion step. The numerical diffusion flux is calculated as

$$\mathbf{H}_{j+\frac{1}{2}} = \frac{a_{j+\frac{1}{2}}^+ a_{j+\frac{1}{2}}^-}{a_{j+\frac{1}{2}}^+ - a_{j+\frac{1}{2}}^-} [\mathbf{U}_{j+\frac{1}{2}}^+ - \mathbf{U}_{j+\frac{1}{2}}^-] S, \quad (17)$$

where the superscripts $+$ and $-$ denote the fluid properties on the right and left sides of the cell surfaces, which are in turn obtained from reconstruction in the two neighboring cells using the same method in the convection step. The one-sided characteristic speeds are denoted as $a_{j+1/2}^+$ and $a_{j+1/2}^-$ based on the Jacobian matrix $\partial \mathbf{F}_{U, i} / \partial \mathbf{U}$.

The viscous term in the momentum equation is discretized in time using the Crank-Nicholson method, while the surface tension term is treated explicitly.

$$\frac{(\rho u_i)^{***} - (\rho u_i)^{**}}{\Delta t} - \frac{1}{2} \frac{\partial \tau_{ij}^{***}}{\partial x_i} = \frac{1}{2} \frac{\partial \tau_{ij}^n}{\partial x_i} + \sigma \kappa \frac{\partial (f)^n}{\partial x_i}, \quad (18)$$

where the superscript *** indicate the variables after incorporating the viscosity-surface-tension step. The curvature κ is computed by the height-function method [16]. The viscous and surface tension terms for the energy are computed similarly, but for each phase separately.

To allow an all-Mach-number capability, the Helmholtz-Poisson equation is solved for the pressure, which is derived from the mixture internal-energy equation in terms of mean pressure (Eq. (11)),

$$\frac{p^{n+1} - p^{***}}{\Delta t} = -(\rho c^2)^{***} \left(\frac{\partial (u_i)^{***}}{\partial x_i} + \Delta t \frac{\partial}{\partial x_i} \left(\frac{1}{\rho} \frac{\partial p}{\partial x_i} \right)^{n+1} \right), \quad (19)$$

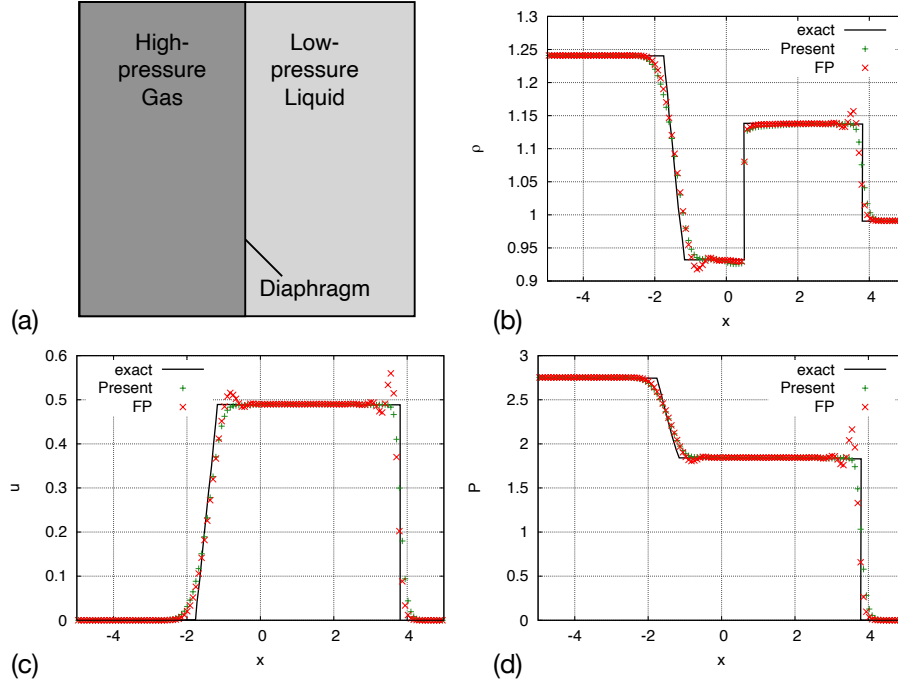


Figure 1. Simulation setup (a) and results of (b) density, (c) velocity, and (d) pressure for the gas-liquid two-phase shocktube problem at $t = 0.2$. The solid lines represent the exact solution, and “FP” represents the results using the method by Fuster and Popinet [7].

where p^{***} is a provisional pressure that accounts for only the convection and viscous terms, computed by the EOS, namely

$$p^{***} = \left[\left(E^{***} - \frac{1}{2} \rho^{***} u_i^{***} u_i^{***} \right) - \frac{\gamma \Pi_\infty}{\gamma - 1} \right] \left(\frac{1}{\gamma - 1} \right)^{-1}. \quad (20)$$

The obtained pressure will be used to correct the velocity and the energy for each phase.

$$u_i^{n+1} = u_i^{***} - \Delta t \left(\frac{1}{\rho} \frac{\partial p}{\partial x_i} \right)^{n+1}. \quad (21)$$

$$(fE_l)^{n+1} = (fE_l)^{***} - \Delta t f \frac{\partial (p u_i)^{n+1}}{\partial x_i}, \quad (\hat{f}E_g)^{n+1} = (\hat{f}E_g)^{***} - \Delta t \hat{f} \frac{\partial (p u_i)^{n+1}}{\partial x_i}. \quad (22)$$

Results and discussion

Two-phase shocktube

The 1D gas-liquid two-phase shocktube problem is employed to test the present method on capturing interfaces separating two different phases. The problem has been used as a model to study underwater explosions [17, 1]. The domain is a square with $L = 10$ and $x = [-5, 5]$. The diaphragm is initially located at $x = 0$. The initial fluid properties are given as

$$\{\rho, u, p, \gamma, \Pi_\infty, f\} = \begin{cases} \{1.241, 0, 2.753, 1.4, 0, 0\} & -5 \leq x \leq 0, \\ \{0.991, 0, 3.059 \times 10^{-4}, 5.5, 1.505, 1\} & 0 \leq x \leq 5. \end{cases} \quad (23)$$

Consistent with former studies, the viscosity and surface tension are neglected in this test. The present results for density, velocity, and pressure are compared with the exact solutions in Fig. 1 and a good agreement is achieved. The numerical oscillations induced by the FP method are profound and are observed not only near the shock but also near the tailing edge of the

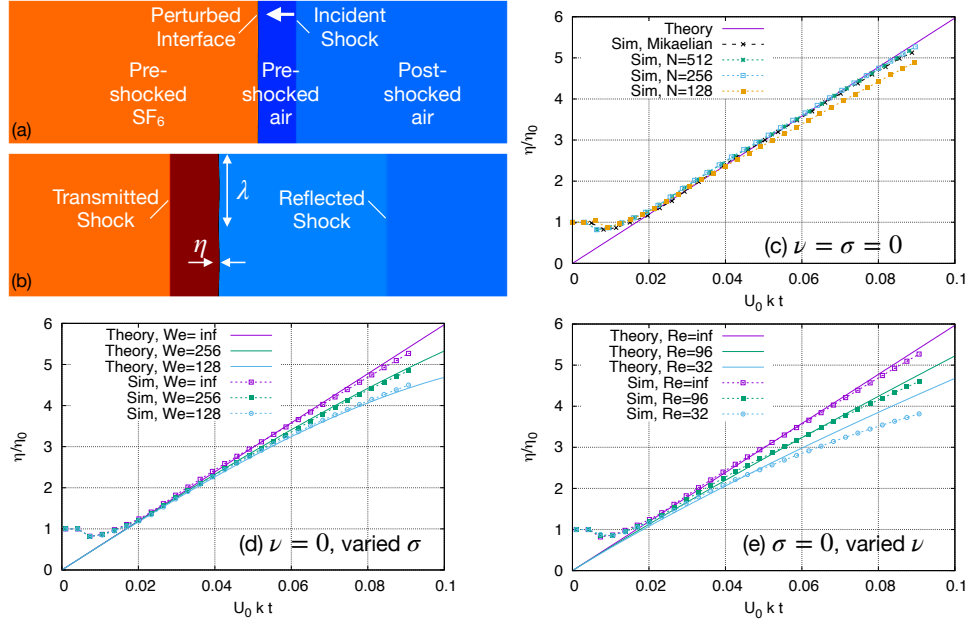


Figure 2. Simulation results for single-mode RMI. (a) Temporal evolutions of the density field. (b) Inviscid case ($\sigma = \nu = 0$) with different mesh resolutions $N = \lambda/\Delta = 128, 256$ and 512 , compared with the simulation results of Mikaelian [20] and the inviscid theory of Richtmyer. (c) Results for $We = \infty, 256, 128$ and $\nu = 0$ compared with the theory of Carles and Popinet [21]. (d) Results for $Re = \infty, 96, 32$ and $\sigma = 0$ compared with the theory of Carles and Popinet [21].

expansion fan. It is also worth noting that, for the present method, the gas-liquid interface is resolved as a genuine discontinuity. Furthermore, the velocity and pressure are continuous at the interface without any numerical oscillations, which is known as an important feature that is not trivial to achieve numerically [18].

Richtmyer-Meshkov instability

The Richtmyer-Meshkov instabilities (RMI) [19] is simulated to examine the present method in resolving the capillary and viscous effects on shock-interface interaction. The RMI is triggered by the shock interaction with a perturbed interface, and it plays an essential role in the interaction between shocks and bubbles/droplets. Here we only consider the linear regime of single-mode RMI. Different Weber We and Reynolds Re numbers are considered.

The simulation setup is shown in Fig. 2(a). A planar air shock moves from right to left toward a perturbed interface separating two immiscible fluids. The incident shock velocity is $u_s = 422.88$ m/s (shock Mach number $M_s = 1.24$). Both fluids are considered as ideal gases, so $\Pi_\infty = 0$. The initial conditions and fluid properties are given as

$$\{\rho, u, p, \gamma, f\} = \begin{cases} \{1.22, 0, 1.013 \times 10^5, 1.4, 0\} & \text{Preshocked fluid 1,} \\ \{2.176, -123.1, 1.649 \times 10^5, 1.4, 0\} & \text{Postshocked fluid 1,} \\ \{6.20, 0, 1.013 \times 10^5, 1.09, 1\} & \text{Preshocked fluid 2,} \end{cases} \quad (24)$$

in SI units. The wavelength and amplitude of the initial perturbation are $\lambda = 3.75$ cm and $\eta_0 = 0.01$ cm, respectively. The post-shocked fluid densities for fluids 1 and 2 are $\rho_{1b} = 11.16$ kg/m³ and $\rho_{2b} = 1.93$ kg/m³, respectively, and the velocity change induced by the shock passage is $\Delta u = 81.1$ m/s. As a result, the Atwood number $A = (\rho_{1b} - \rho_{2b})/(\rho_{1b} + \rho_{2b})(1 - \Delta u/u_s) = 0.705$. The Richtmyer velocity, $U_0 = \eta_0 \Delta u k A = 0.77$ m/s. When surface tension and viscosities are zero, the selected parameters are the same as the simulation of Mikaelian [20]. The surface tension and viscosities are then arbitrarily varied to study the effect of We and Re on the development of RMI. The simulation results are validated against the linear

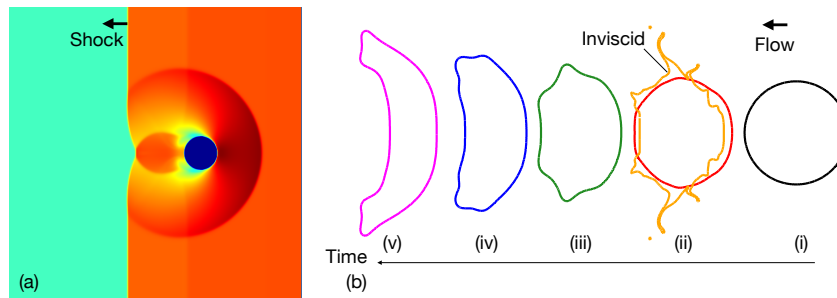


Figure 3. Simulation results for shock-drop interaction. (a) Gas density and (b) temporal evolution of drop morphology.

theories of Carles and Popinet [21]. The Weber and Reynolds numbers are defined as $We = (\rho_{1b} + \rho_{2b})(\Delta u)^2/k\sigma$ and $Re = \Delta u/k\nu$. For convenience we simply set $\nu_1 = \nu_2 = \nu$ and $\lambda_v = 0$. Two different values are considered for We and Re , respectively, namely $We = 128, 256$ and $Re = 32, 96$. The results are summarized in Fig. 2.

The present simulation results for the inviscid limit ($\nu = 0$, $\sigma = 0$) with different mesh resolutions (the number of cells per wavelength $N = \lambda/\Delta = 128, 256$, and 512) are shown in Fig. 2(a). It is observed that the simulation results converge for $N = 256$ and agree well with the simulation results of Mikaelian [20] and also the theory of Richtmyer [19]. For the linear stability theory, the perturbation amplitude grows right after the impulsive acceleration is imposed, while in simulation the perturbation amplitude first decreases due to the shock compression and then grows linearly. Here the theoretical results are plotted as $\eta/\eta_0 - 1$ and the simulation results are shifted in time so that the two have the same starting time for the linear growth. It is measured that the computed perturbation linear growth rate $d\eta/dt = 0.74$ m/s, which is very close to the theoretical prediction, *i.e.*, the Richtmyer velocity $U_0 = 0.77$ m/s. The temporal evolutions of the density field for the inviscid case and $N = 256$ are shown Fig. 2(d), where the transmitted and reflected shocks and the growth of the interface perturbation are well resolved.

The simulation results for finite We and Re are presented in Figs. 2(b) and (c). The effects of surface tension and viscosity on RMI are similar, *i.e.*, the growth rate decreases over time. The smaller the We or Re , the larger the decrease in the growth rate. The present simulation results agree well with the theory of Carles and Popinet [21] for the different values of We and Re considered here. As the theory is valid only for small t , the simulation results deviate from the theoretical predictions at later time.

Shock-drop interaction

The interaction between a planar air shock wave and a 2D water drop is also simulated. The experiment of Igra and Takayama [22] is simulated and the results agree well with the experiment. The We and Re for the 2D drop in the experiment of Igra and Takayama are very large, so the viscous and capillary effects on the short-term behavior are negligible. Alternatively, we have simulated a smaller drop to illustrate the effect of viscosity and surface tension on shock-drop interaction and the subsequent breakup. The water drop of diameter is $D_0 = 15.8$ μm and the planar shock Mach number is $M_s = 1.47$. The postshocked gas density and velocity are 2.176 kg/m^3 and 225.57 m/s, respectively, correspondingly $We = 25$ and $Re = 431$. The gas density contour just after the passage of the shock is shown in Fig. 3(a). The reflected and refracted shocks can be identified, which are found to agree with the experimental results [22]. The temporal evolution of the drop surface is shown in Fig. 3(b). It can be seen that the circular drop is first compressed from both upstream and downstream sides to a disk. Then the disk bends, forming a backward facing bag. For the frame (ii), the drop shape obtained from an inviscid simulation ($\mu_g = \mu_l = \sigma = 0$) is also shown for comparison. It is clear that the viscous and capillary forces must be incorporated to capture correct deformation of the drop.

Conclusions

A new numerical method has been developed to simulate compressible interfacial multiphase flows that involve shock interaction with sharp interfaces. The present numerical method is first tested by the two-phase shocktube problem. The simulation results agree well with the exact solution, with spurious oscillations near the shock and tail of expansion fan effectively suppressed while the interface is captured as sharp interface. Furthermore, the linear single-mode Richtmyer-Meshkov instabilities for different Weber and Reynolds numbers are simulated to examine the capability of the present method in accurately capturing the capillary and viscous effects on shock-interface interactions. The simulation results are compared with linear stability theory and a good agreement is achieved. Finally, the interaction between a shock and a 2D drop with moderate Weber and Reynolds numbers is considered. It is shown that the viscous and capillary forces can be important to the shock-induced drop deformation.

Acknowledgements

This research was supported by the National Science Foundation (#1853193). The authors also acknowledge XSEDE and TACC for providing the computational resources. We also thank Dr. Daniel Fuster for sharing his code and helpful discussions.

References

- [1] Johnsen, E. and Colonius, T. "Implementation of WENO schemes in compressible multi-component flow problems." *J. Comput. Phys.* Vol. 219 (2006): pp. 715–732.
- [2] Meng, J. C. and Colonius, T. "Numerical simulations of the early stages of high-speed droplet breakup." *Shock Waves* Vol. 25 (2015): pp. 399–414.
- [3] Meng, J. C. and Colonius, T. "Numerical simulation of the aerobreakup of a water droplet." *J. Fluid Mech.* Vol. 835 (2018): pp. 1108–1135.
- [4] Schmidmayer, K., Petitpas, F., Daniel, E., Favrie, N. and Gavriluk, S. "A model and numerical method for compressible flows with capillary effects." *J. Comput. Phys.* Vol. 334 (2017): pp. 468–496.
- [5] Garrick, D. P., Hagen, W. A. and Regele, J. D. "An interface capturing scheme for modeling atomization in compressible flows." *J. Comput. Phys.* Vol. 344 (2017): pp. 260–280.
- [6] Garrick, D. P., Owkes, M. and Regele, J. D. "A finite-volume HLLC-based scheme for compressible interfacial flows with surface tension." *J. Comput. Phys.* Vol. 339 (2017): pp. 46–67.
- [7] Fuster, D. and Popinet, S. "An all-Mach method for the simulation of bubble dynamics problems in the presence of surface tension." *J. Comput. Phys.* Vol. 374 (2018): pp. 752–768.
- [8] Corot, T., Hoch, P. and Labourasse, E. "Surface tension for compressible fluids in ALE framework." *J. Comput. Phys.* Vol. 407 (2020): p. 109247.
- [9] Saurel, R. and Pantano, C. "Diffuse-interface capturing methods for compressible two-phase flows." *Annu. Rev. Fluid Mech.* Vol. 50 (2018): pp. 105–130.
- [10] Xiao, F., Honma, Y. and Kono, T. "A simple algebraic interface capturing scheme using hyperbolic tangent function." *Int. J. Numer. Meth. Fluids* Vol. 48 (2005): pp. 1023–1040.
- [11] Kurganov, A. and Tadmor, E. "New high-resolution central schemes for nonlinear conservation laws and convection–diffusion equations." *J. Comput. Phys.* Vol. 160 (2000): pp. 241–282.
- [12] Marsh, S. P. *LASL shock Hugoniot data*. Vol. 5. University of California Press (1980).
- [13] Scardovelli, R. and Zaleski, S. "Direct numerical simulation of free-surface and interfacial flow." *Annu. Rev. Fluid Mech.* Vol. 31 (1999): pp. 567–603.
- [14] Arrufat, T., Cialesi-Esposito, M., Fuster, D., Ling, Y., Malan, L., Pal, S., Scardovelli, R., Tryggvason, G. and Zaleski, S. "A momentum-conserving, consistent, Volume-of-Fluid method for incompressible flow on staggered grids." *Comput. Fluids* Vol. 215 (2020): p.

104785.

- [15] Bell, J. B., Colella, P. and Glaz, H. M. "A second-order projection method for the incompressible Navier-Stokes equations." *J. Comput. Phys.* Vol. 85 (1989): pp. 257–283.
- [16] Popinet, S. "An accurate adaptive solver for surface-tension-driven interfacial flows." *J. Comput. Phys.* Vol. 228 No. 16 (2009): pp. 5838–5866.
- [17] Shyue, K. "An efficient shock-capturing algorithm for compressible multicomponent problems." *J. Comput. Phys.* Vol. 142 (1998): pp. 208–242.
- [18] Abgrall, R and Karni, S. "Computations of compressible multifluids." *J. Comput. Phys.* Vol. 169 (2001): pp. 594–623.
- [19] Richtmyer, R. D. "Taylor instability in a shock acceleration of compressible fluids." *Commun. Pur. Appl. Math.* Vol. 13 (1960): pp. 297–319.
- [20] Mikaelian, K. O. "Growth rate of the Richtmyer-Meshkov instability at shocked interfaces." *Phys. Rev. Lett.* Vol. 71 (1993): p. 2903.
- [21] Carles, P. and Popinet, S. "The effect of viscosity, surface tension and non-linearity on Richtmyer–Meshkov instability." *Eur. J. Mech. B/Fluids* Vol. 21 (2002): pp. 511–526.
- [22] Igra, D. and Takayama, K. "Numerical simulation of shock wave interaction with a water column." *Shock Waves* Vol. 11 (2001): pp. 219–228.